#Author postprint version#

Ecological signal in the size and shape of marine amniote teeth

Valentin Fischer[1,*], Rebecca F. Bennion[1,2], Davide Foffa[3,4,5], Jamie A. MacLaren[1,6], Matthew R. McCurry[7,8,9], Keegan M. Melstrom[10,11], Nathalie Bardet[12]

[1] Evolution & Diversity Dynamics Lab, Université de Liège, 4000 Liège, Belgium.
[2] Palaeobiosphere evolution, Royal Belgian Institute of Natural Sciences, Brussels Belgium.
[3] Department of Natural Sciences, National Museums Scotland, Edinburgh EH1 1JF, United Kingdom.
[4] School of Geography, Earth and Environmental Sciences, University of Birmingham, Birmingham B15 2TT, United Kingdom.
[5] Department of Geosciences, Virginia Tech, Blacksburg, Virginia 24061, USA.
[6] Functional Morphology Lab, Department of Biology, Universiteit Antwerpen, 2610 Antwerpen, Belgium.
[7] Australian Museum Research Institute, Sydney, New South Wales 2010, Australia.
[8] Earth and Sustainability Science Research Centre, School of Biological, Earth and Environmental Sciences (BEES), University of New South Wales, Kensington, New South Wales 2052, Australia.
[9] Paleobiology, National Museum of Natural History, Smithsonian Institution, Washington, DC 20560, USA.
[10] Engineering and Science Division, Rose State College, Midwest City, OK 73110, USA.
[11] Dinosaur Institute, Natural History Museum of Los Angeles County, Los Angeles, CA, 90007 USA.
[12] Centre de Recherche en Paléontologie - Paris, CNRS-MNHN-SU, Muséum National d'Histoire Naturelle, 75005 Paris, France.

* corresponding author: Valentin Fischer, v.fischer@uliege.be

Classification: Biological Sciences; Ecology.

Keywords: high-density morphometrics; marine reptiles; Cetacea; feeding guilds; palaeoecology

ABSTRACT

Amniotes have been a major component of marine trophic chains from the beginning of the Triassic to present day, with hundreds of species. However, inferences of their (palaeo)ecology have mostly been qualitative, making it difficult to track how dietary niches have changed through time and across clades. Here, we tackle this issue by applying a novel geometric morphometric protocol to 3D models of tooth crowns across a wide range of raptorial marine amniotes. Our results highlight the phenomenon of dental simplification and widespread convergence in marine amniotes, limiting the range of tooth crown morphologies. Importantly, we quantitatively demonstrate that tooth crown shape and size are strongly associated with diet, whereas crown surface complexity is not. The maximal range of tooth shapes in both mammals and reptiles is seen in medium-sized taxa; large crowns are simple and restricted to a fraction of the morphospace. We recognise four principle raptorial guilds within toothed marine amniotes (durophages, generalists, flesh cutters, and flesh piercers). Moreover, even though all these feeding guilds have been convergently colonised over the last 200 million years, a series of dental morphologies are unique to the Mesozoic period, probably reflecting a distinct ecosystem structure.

INTRODUCTION

Since the Permian, more than sixty amniote lineages (predominantly diapsid reptiles and placental mammals) independently transitioned from terrestrial to aquatic environments [1,2]. The strong constraints of the aquatic medium channelled phenotypic evolution and forced widespread convergences, notably in body shape [3], physiology [4,5], and feeding strategies [6,7]. No matter the ancestral complexity, the teeth of most marine amniotes appear simplified towards a conical or bulbous shape, which makes their functional interpretation fairly straightforward [6,8]. As such, marine tetrapod teeth have been extensively used as a proxy for the ecological niche of their bearers, yielding important insights into the composition of ancient marine ecosystems [6,9].

However, the dominant frameworks linking tooth shape with diet do not take tooth size into account [6,8], despite appearing strongly linked to the diet of extant marine amniotes (e.g. cetaceans [10]). Being qualitative [6], or essentially based on a few discrete features [8], these frameworks do not specifically use crown morphology such as flat surfaces (e.g. the subtrihedral teeth of thalassophonean pliosaurids [11,12]), carinae, apical cusplets (e.g. the mosasaurine mosasauroid *Globidens* [9]), and the direction of curvature. More recent analyses of marine reptile teeth have started incorporating size [13,14] or ornamentation, but discretised [12,15]. This study presents a new, quantitative, and almost fully-automated protocol that addresses all these issues at once. The method uses geometric morphometrics [16–18], with an element of automatic pseudo-landmarking [19], designed to accurately sample tooth shape after placing minimal homologous landmarks per tooth. We apply this protocol

to a new dataset of three-dimensional (3D) tooth crown models of 54 taxa of obligate marine amniotes, both extinct and extant. We then use these data to: (i) analyse interplay between tooth shape, tooth size, gut content, and dental surface complexity in marine tetrapods and (ii) propose a new framework to classify these organisms into feeding guilds and infer their trophic role. Furthermore, our new protocol can easily be applied to explore shape variation and disparity in a variety of simple structures, opening new research avenues.

MATERIAL & METHODS

Morphological data and sampling

We sampled a total 54 taxa of extinct and extant raptorial, fully-toothed, aquatic amniotes, representing cetaceans, sauropterygians, mosasaurid squamates, archosaurians, and ichthyosaurians, and covering most of the marginal (i.e. not palatal or pterygoid) tooth shapes present in these groups. We did not incorporate crowns from taxa with incomplete dentition such as the sperm whale *Physeter macrocephalus*, nor from dental plates, where the tight fit of palatal teeth results in polygonal crowns such as in placodont sauropterygians (marginal teeth from placodonts are however incorporated in our dataset). Nevertheless, our protocol (see below) works very well on these shapes, as well as other conical objects (Fig. 1, S1).

We sampled the best-preserved, unworn teeth within a narrow region located in the middle of the snout (i.e. half of pre-orbital snout length), where the teeth are usually large and worn [20,21], indicating these were often used in food procurement. Our sampling strategy allowed teeth with minor breaks in the enamel to be incorporated; see Table S1 for all details. For isolated teeth, we selected teeth matching the tooth shape expected in that region of the snout. One exception is the highly heterodont mosasaurid *Globidens*, for which we also selected one distal tooth in addition to a tooth from the mesial third of the mandible. Two worn teeth have also been selected (one belonging to *Orcinus orca* and one belonging to *Pliosaurus* sp.) to visualise how tooth wear affects position in morphospaces. By convention, we sampled right dentary teeth. In specimens where the teeth of this region were not well preserved, the strong left-right symmetry in dental elements [22] permitted the sampling of left dentary or maxillary teeth; a mirroring algorithm was applied wherever necessary. This resulted in a total of 56 tooth crowns. Most were digitised using a laser scanner (Creaform Handyscan 300), at a 0.2 mm resolution. Others have been obtained as CT-scans or photogrammetric models from published supplementary data, MorphoSource, or colleagues; see tables S1, S2 for metadata.

Size and dietary categories

We gathered two measurements from the same specimens sampled for their tooth crowns, when possible: mandible length (anterior tip of the symphysis to posterior margin of the glenoid cavity) and interglenoid distance (distance between medial

surfaces of the mandibular glenoids, or the corresponding cranial elements of the jaw joint when needed), both rounded to the nearest millimetre, using the software Meshlab [23]. The latter represents a proxy for the diameter of the gullet, i.e., the upper bound of the prey items (whole or fractionated) that can be swallowed. We also calculated crown height as the Euclidean distance between the apex (fixed landmark 1) and the centre of the base of the crown (taken at the mean point between fixed landmarks 4 [distal base of the crown] and 5 [mesial base of the crown]).

Gastric content reported in a specimen is generalised to the generic level if the species in question have similar mandible lengths and crown morphologies. For example, the gastric content reported for *Mosasaurus missouriensis* [24] is generalised to *Mosasaurus hoffmanni* and *Mosasaurus lemmonieri* but the gastric content reported for *Prognathodon overtoni* [24] is not generalised to *Prognathodon currii* (tooth crowns clearly different in shape) or *Prognathodon solvayi* (notably smaller skull size). The dietary categories we establish ('flesh, large', 'flesh, medium', 'flesh, small', 'shelled, large', and 'shelled, small'; see Table S3 for details) take the variety of prey items into account, focussing on their sizes, hardness, and trophic positions rather than phylogenetic relatedness (see Table S4 for the data).

High-density geometric morphometrics and morphospace occupation

The tooth crowns of raptorial marine amniotes are essentially conical (except in carnivoran mammals), leaving few homologous points that can be landmarked. Moreover, a high number of surface landmarks is needed to fully capture peculiar, functionally important traits such as carinae and flat surfaces. In this paper, we establish a new protocol mixing pseudolandmarking [25] into high-density landmarking procedures. This procedure requires placement of just five fixed 3D landmarks on a 3D model of each tooth crown, and then automatically samples thousands of points on the crown surface in R [26]. The procedure is summarised in Fig. 1 and a detailed step-by-step guide is provided in supplementary information. The surface of a simple shape (here a 3D dome) is landmarked automatically (2000 surface semi-landmarks) by sampling the coordinates of the triangles composing this shape; this part of the protocol is borrowed from pseudolandmarking techniques. Then, using the geomorph v4.0.3 [27] and Morpho v2.9 [28] packages, an atlas is created and is used to patch the 2000 surface semi-landmarks onto each crown model. A Generalised Procrustes Superimposition (GPA) is then called to eliminate the size and positioning factors and then a Principal Component analysis (PCA) is applied on the GPA coordinates to produce morphospaces. Density-based macroevolutionary landscape are then produced using the method explained in Fischer et al. [29]. Newly digitized models are deposited on Morphosource (https://www.morphosource.org/projects/000435369). All 3D tooth crown models and their fixed landmark coordinates, as well as the R script (including automatic cropping of crown models for OPCR analyses) are openly available in the Supplementary Information and ORBi (https://hdl.handle.net/2268/293921).

Statistical tests

Correlations were tested for by regressing log-transformed measurements against one another. The significance of crown size differences in terms of dietary categories and shape was tested using Wilcoxon-Mann-Whitney test. A multivariate analysis of variance (MANOVA) was used in a pairwise manner to test for morphological differences between feeding guilds initially established by Massare [6] (see also [9,13,30] for detailed explanations of these guilds); separate MANOVAs analysed the shape differences between 'small' and 'large' crowns (defined by fossilised gut content; threshold ~20 mm, see Results). MANOVAs were performed using the PC axes accounting for >1% of the total variance (i.e. the first four, which together explain >95% of the total variance).

OPCR

Orientation Patch Count Rotated (OPCR) quantifies surface complexity by counting the number of patches with a given orientation in a 3D model [e.g. 31] and has been successfully applied to amniote dentition [e.g. 32]. To ensure that the OPCR and high-density geometric morphometric analyses sample the exact same portion of the 3D models, we wrote a short script that automatically crops each 3D model according to a plane defined by three of the fixed landmarks located at the base of the crown and exports this new model as 3D mesh. Each resultant mesh was then simplified to 1000 triangles using MeshLab v 2020.07 [23], with the apex aligned along the z-axis. We used the molaR_Batch function (OPCr_minimum_faces = 3 and 5) from the package molaR v4.5 [31] to compute surface complexity.

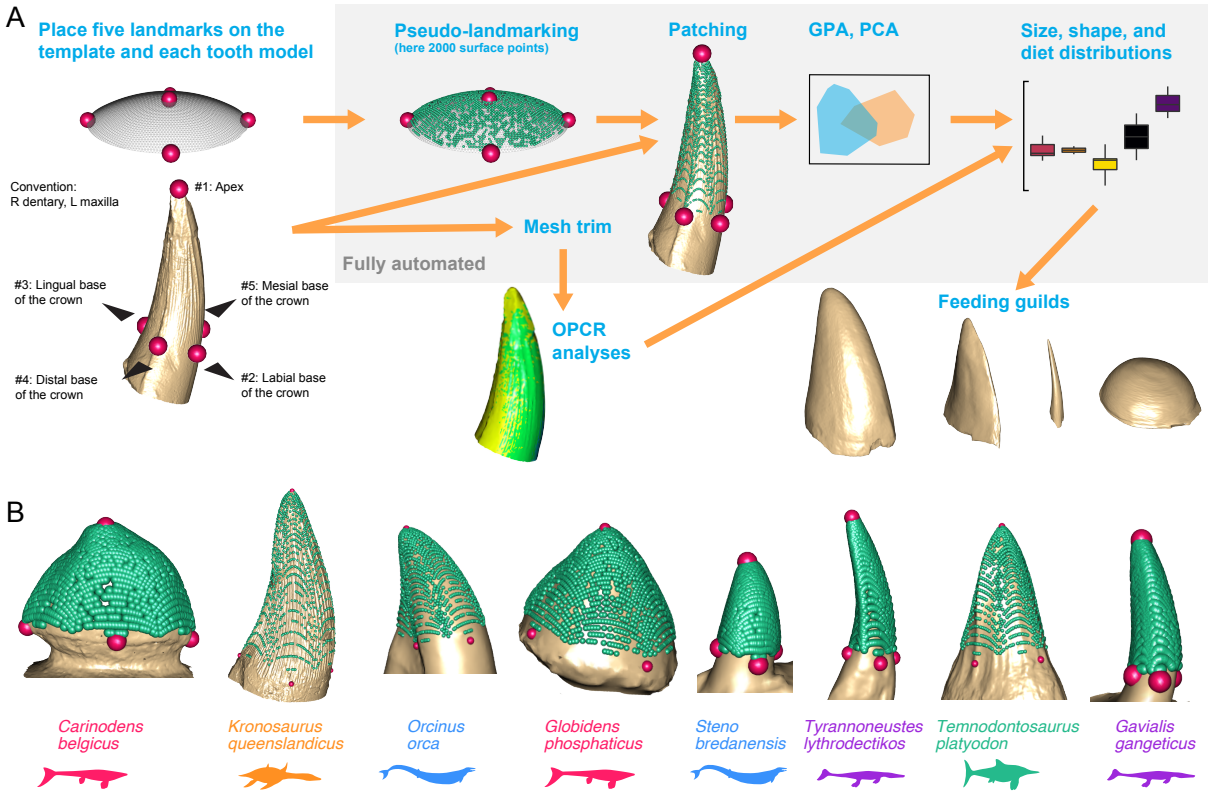

Figure 1. High-density shape sampling protocol. **A**, Steps of the high-density geometric morphometrics procedure; the part in the grey background is fully automated. The crowns under "Feeding guilds" have been generated by thin-plate spline of PC1 and PC2 extremes (see Fig. 2). **B**, Example of 3D crown meshes with their fixed landmarks (5, in pinkish red colour) and their surface semi-landmarks (2000, in green sea colour), not to scale. The silhouettes are clade- not species-specific. Abbreviations: GPA: Generalised Procrustes Superimposition; PCA: Principal Component Analysis.

RESULTS

Morphospace occupation and crown complexity

Our novel procedure can sample marine amniote crown shape extensively (Figs. 1, S1), and can notably capture morphological details such as some of the apicobasal ridges of pliosaurids (Fig. S2). Reduction of dimensionality through principal component analysis (PCA) captures 90.79% of the variance with just two axes, the first axis accounting for 86.73% (Figs. 2, S3). The first principal component axis (PC1) describes the aspect ratio of the tooth crown, going from the bulbous teeth of globidensine mosasaurids and placodonts (highest positive PC1) to the recurved, needle-like teeth of long-necked plesiosaurians and early thalattosuchians (highly negative PC1); morphospace occupation per species is detailed in Fig S3 and can also be visualised interactively (see R script in supplementary Information). The second principal component axis (PC2) describes the labiolingual compression of the tooth crown and the direction of tooth curvature: taxa with labiolingually-flattened and distally-recurved crowns such as mosasaurids and archaeocetes occupy the maximal

positive values whereas taxa with circular crowns directed lingually (such as delphinoids) occupy the maximal negative values. In our sample, the flatness of the crown often associates with the presence of carinae (i.e. sharp cutting edges), so this axis carries an important functional signal. The third principal component axis (PC3) only accounts for 2.77% of the variance and captures slight variations of the direction of curvature as well (mesial vs. mesiodistal). All the other PC axes (53 out of 56) account for less than 2% of the variance (Table S5) and will not be described. A large majority of teeth (≈75%), encompassing all main clades, cluster in a region between -0.25 and 0.0 on PC1 and close to 0.0 on PC2, representing conical and slightly labio-lingually-compressed crowns (Fig. 2A-B; Fig. S3). This numerically confirms that most marine amniotes have fairly simple and similarly-shaped tooth crowns. This clustering also results in unexplored dental morphologies, notably in high positive values along PC2, which contain crowns which are strongly labiolingually compressed. The region in between clear durophages (placodont sauropterygians and globidensine mosasaurids) and 'conical' toothed taxa is also sparsely occupied, with few taxa exhibiting straight, high dome-shaped teeth. Only three specimens occupy this region, and two of them are very large: the mosasaurine *Prognathodon currii*, which evolved a very large size and a crushing diet from small, flesh-eating ancestors [9] and the gigantic physeteroid *Livyatan melvillei*, which possesses the largest skull ever recorded for a raptorial amniote [33]. The third specimen in that region is a worn tooth of the delphinid *Orcinus orca*. Our results show that the effect of apical wear can be strong, transforming the piercing conical crowns of *Orcinus orca* into a morphology close to that of some shell-crushing mosasaurids. Despite having active tooth replacement [34], a similar trend is observed in *Pliosaurus*, travelling about $1/5^{th}$ of the length of PC1 towards positive values because of apical wear (Fig. 2A).

We tested how the feeding guilds first established by Massare [6] correlate with our new shape data. The 'Crush' guild appears clearly separated from the others (Fig. S4). If only the first four axes of the PCA are used (accounting for >95% of the total variance), the 'Smash' and 'Crunch' guilds are recovered as significantly distinct (MANOVA p-value < 0.05), being separated along PC2, as are 'Cut' and 'Pierce' guilds (MANOVA p-value < 0.05). The main issue lies in the 'General' guild(s), which cannot be distinguished from the 'Pierce' guild (MANOVA p-value = 0.05623) nor from the 'Cut' guild (MANOVA p-value = 0.05137).

Our OPCR results pair well with the density of morphospace occupation (Fig. 2A-B) in indicating a strong tendency towards simple conical crown morphologies. The range of OPCR values is generally low, similar to non-herbivorous, non-multicusped lizards [22,35]. Only a few taxa exhibit high values, although this is likely due to damaged enamel (e.g. *Livyatan melvillei*) or variations in tooth size and resolution of scans (e.g. very large ridged teeth of *Kronosaurus queenslandicus*/*Eiectus longmani*). Values for larger taxa are thus relatively high compared to smaller species, because the resolution of laser and CT-scanning is scale-dependent. Nevertheless, the important

morphological variation in marine amniote tooth shapes pairs with very little difference in their surface complexity, irrespective of scale.

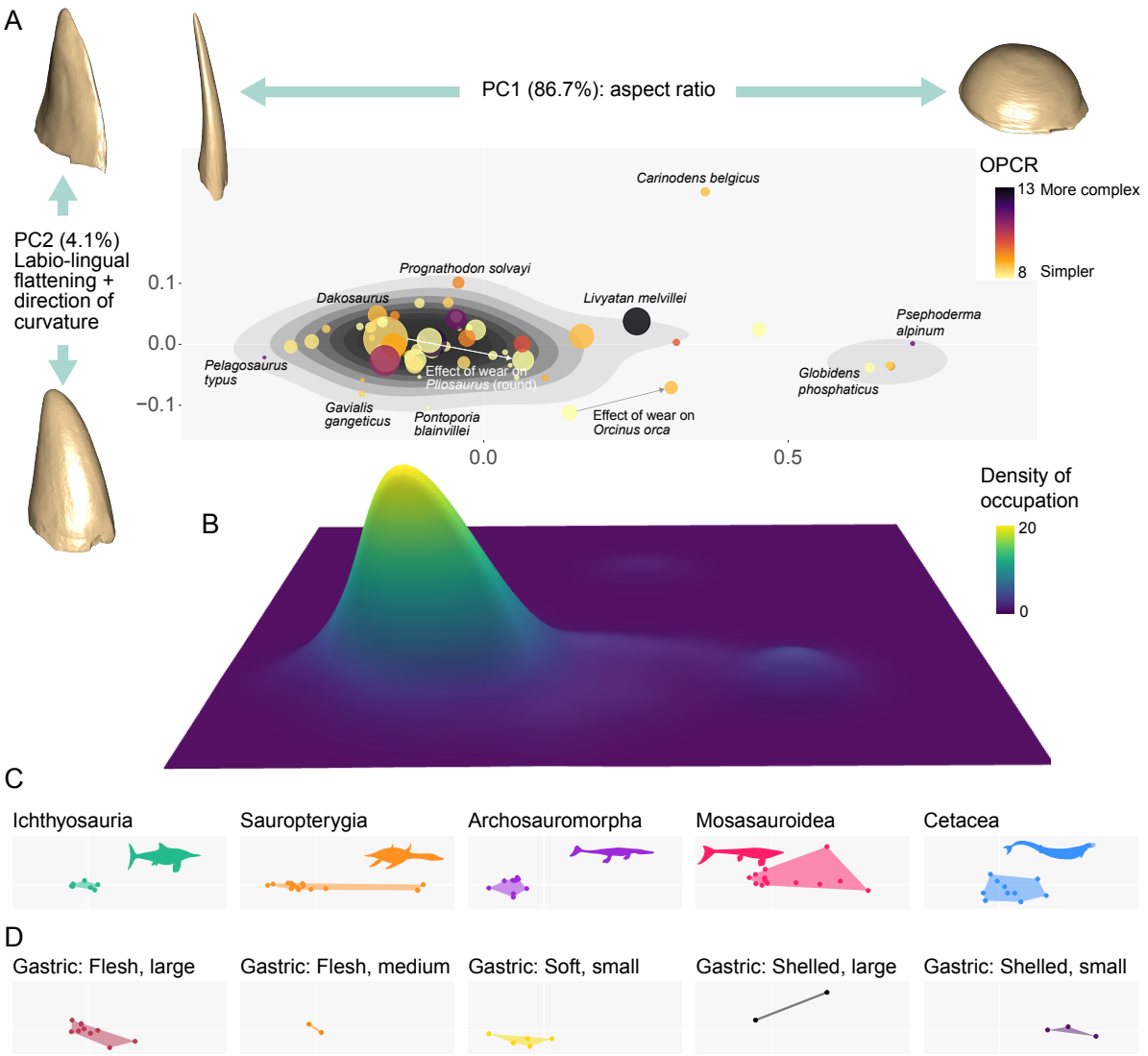

Figure 2. Dental morphospace occupation by raptorial marine amniotes. **A**, morphospace occupation visualised by the first two axes of the PCA. The diameter of each dot is directly proportional to centroid size. The colour of each dot is the corresponding OPCR value for this 3D mesh. See also the effect of apical wear on *Pliosaurus* and *Orcinus orca* (white and grey arrows, respectively). Density of morphospace occupation is visualised by shades of grey (darker = higher density; see also B). We visualised the morphological features captured by the axes of the PCA by predicting the shape at the extremes of each axis multiplied by 1.2, thus providing a slightly more exaggerated shape than the taxa analysed. We then warping the 3D mesh of *Mosasaurus hoffmanni* (ULg PA 25119a) to match the four sets of predicted landmarks using a thin-plate spline function. **B**, Density of morphospace occupation visualised as a 3D object, showing a clear majority of raptorial marine amniote teeth have a similar morphology. **C**, morphospace occupation (PC1, PC2) per clade. **D**, morphospace occupation (PC1, PC2) per gastric content.

Distribution of size and gastric contents

Crown size is not distributed randomly: both the centroid size and the apicobasal height of the crown are positively correlated with mandible length (centroid size: R^2 = 0.5424, p-value < 0.0001; crown height: R^2 = 0.7068, p-value < 0.0001) and interglenoid distance (a proxy for gullet diameter) (centroid size: R^2 = 0.6828, p-value < 0.0001; crown height: R^2 = 0.4832, p-value < 0.001) (Fig. S5). The distribution of crown sizes along PC1 and PC2 is not random either: most teeth are clustered close to the origin of both axes, indicating that a majority of teeth have unspecialised, 'common' overall morphologies. This is especially evident for large teeth (i.e., crown height > 20 mm); the range of PC1 and PC2 values occupied by these teeth is much smaller (53.4% and 58.9% of the total spread, respectively) and their disparity is significantly smaller than that of small crowns (Wilcoxon-Mann-Whitney p-value < 0.0001; Fig. S6). This indicates that large teeth are usually simple in morphology; more shape variation is seen for crown sizes between 5 and 20 mm, i.e., small to medium-sized taxa (Figs. 3, S5).

The dietary categories deduced from fossilised gut content can be discriminated using a combination of aspect ratio (PC1), curvature (PC2), and crown size (Fig. 3). Only two data points are available for the categories 'flesh, medium' and 'shelled, large', and each contain taxa already present in other dietary categories and will not be discussed here. The aspect ratio alone isolates durophages from large fleshy prey eaters (Wilcoxon-Mann-Whitney p-value < 0.05) and durophages from small fish/squid specialists (Wilcoxon-Mann-Whitney p-value < 0.05), [6] but not large fleshy prey from small fish/squid specialists (Wilcoxon-Mann-Whitney p-value = 0.3097). Tooth crown curvature (PC2) separates small fish/squid specialists from the rest of the dataset, whereas crown size separates large fleshy prey eaters from fish/squid specialists (Fig. 3) (Wilcoxon-Mann-Whitney p-value < 0.001). OPCR values do not correlate with dietary categories, as would be expected given the drivers of that signal in our dataset (see above). Because crown size correlates with gullet diameter and both crown size and shape correlate with diet (Figs. 3, S5), we posit that the combination of crown shape (PC1 and PC2) and crown size forms a solid basis to define feeding guilds, and to analyse trophic diversity in raptorial marine amniotes.

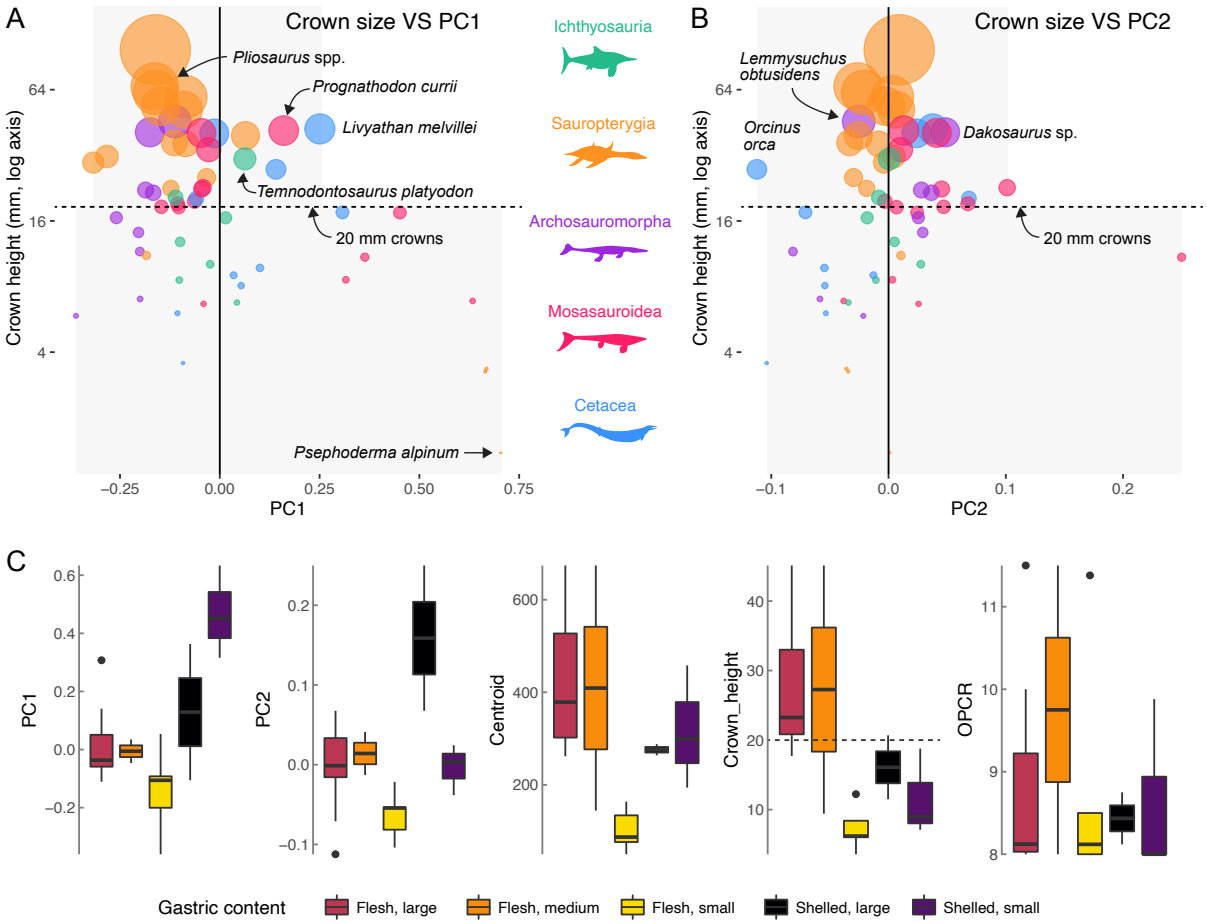

Figure 3. Distribution of size and shape. **A**, Distribution of crown height (log) against PC1. **B**, Distribution of crown height (log) against PC2. The dot size is directly proportional to crown height. In A and B, the range of PC values covered by large and small crowns is indicated by a grey background. This range is much smaller for large (>20mm, above the dotted line) crowns. **C**, Distribution of PC values, centroid sizes, crown heights, and OPCR values per gastric content category as box plots.

DISCUSSION

(a) Large predators have simple teeth

For more than 30 years, teeth have been intensively utilised to infer the palaeoecology of marine amniotes [6,8,9,13,36], based largely on the seminal paper of Massare which established a canvas linking tooth shape with prey preference [6]. However, this essentially qualitative canvas mixes diet with behaviour (e.g. the difference between ‘smash’ and ‘crunch’ guilds) and relies – at times – on data that is difficult to generalise to most marine amniotes [37]. For example, the tooth shape of *Physeter macrocephalus* is seen as indicative of a squid-rich diet in that canvas, despite evidence that the lower dentition does not play an active role in feeding [38], alongside an edentulous upper jaw and a diet including the largest marine invertebrate that has ever evolved [e.g. 39]. A series of tooth morphologies do not fit within ‘Massare’s triangle’ (even if modifications have been attempted [9] as well as thorough attempts to retrofit Massare’s guilds into quantitative frameworks [13]), and – perhaps most

importantly – crucial functional features such as tooth size and the direction of curvature of the tooth crown (distally vs. lingually) are not considered. As an example in this study, the teeth of the Middle Jurassic pliosaurid *Liopleurodon ferox* – regarded as an apex predator / hypercarnivore [40] – are not that different in shape from those of the near-obligately piscivorous gharial (*Gavialis gangeticus*) (Fig. 2A). However, the teeth of *Liopleurodon* are nearly six times larger than those of *Gavialis*, resulting in teeth which would very likely behave differently when used against prey, recalling the concept of 'functional heterodonty' [41]. Similarly, whereas the Early Jurassic ichthyosaurians *Ichthyosaurus* (≈ 3 m long) and *Temnodontosaurus trigonodon* (≈ 8 m long) have relatively similar tooth morphologies [42,43], their gut contents are distinct: fish scales and cephalopod hooklets in *Ichthyosaurus* [6,44] and marine reptiles and cephalopod hooklets in *Temnodontosaurus trigonodon* [45]. Understanding diet through the prism of size instead of just crown shape reconciles records of extant orcas still able to hunt large vertebrate prey despite having rounded, worn (but still large) teeth [46,47].

Our gastric content data confirms that diet correlates with crown size (Fig. 3), which itself correlates with gullet diameter (Fig. S5). A threshold separating animals able to consume large, fleshy, vertebrate prey (the so-called 'top predators') seems to occur for crown size > 20 mm in height (Fig. 3). This size boundary also coincides with a strong reduction in the range of crown morphologies (Fig. 3); above this threshold, all crowns are conical and weakly recurved, often lingually or distolingually, and carinae gradually disappear as crown size increases. From a functional point of view, we posit that the range of possible prey items correlates with crown size; once a fairly straight crown reaches 30-50 mm in height, it will likely be able to damage any kind of possible prey item if enough bite force is applied; this is why it is unsurprising to find cephalopod hooklets alongside marine reptiles in the gut of *Temnodontosaurus* [45]. In parallel, larger body size in active raptorial predators often requires a larger energy intake [e.g. 48], which makes hunting small prey items with low energetic reward less beneficial for these taxa, even though their tooth shape is not necessarily ill-suited for this task. We hypothesise that this increase in dietary possibilities with increasing tooth size (and, to a certain extent, body size) relaxes specialisation pressures on crown shape, resulting in less deviation from simple conical morphologies (Figs 3, S6). These results also suggest that marine amniotes could potentially colonise new niches by changing their tooth (and body) size and not necessarily the shape of their teeth.

Deviations from a simple conical crown (i.e. larger range of shapes along PC axes, as well as carinae and serrations) appear especially frequent for crowns ranging from 5 to 20 mm in height (Figs. 3, S6), suggesting that stronger evolutionary pressures might drive dental differentiation in smaller taxa [49]. Our results make it clear that an explicit incorporation of absolute tooth size (or 'the size of killing/grasping device relative to prey size') is crucial to infer the palaeoecology of extinct marine amniotes and needs to have an influence in guild definitions.

(b) Four main raptorial feeding guilds

We propose four discernible guilds for raptorial aquatic amniotes: durophages, generalists, flesh piercers, and flesh cutters. Generalists have the widest range of food options and the breadth of the generalist guild varies with tooth size. While restricted to a subset of the positive values of PC1 (i.e. conical, slightly recurved teeth with crown height/basal diameter ratio often ranging from 1.2 to 2.7) for small and medium sized teeth, we consider that most taxa with conical crowns larger than 20 mm high belong to the generalist guild (orcas, *Temnodontosaurus*, pliosaurids, many mosasauroids, etc.). As shown above (Fig. 3), the range of shapes above that threshold is low anyway. Durophages have low, bulbous teeth (aspect ratio <1.4 and often <0.7) which resist strong apicobasal compression, ideal for breaking the external protection of hard-shelled animals [6]. Small-prey flesh piercers and flesh cutters both have dental adaptations that presumably help them to enter flesh such as pointed apices, high aspect ratio, and apicobasal ridges. A key difference lies in ornamentation, as flesh cutters usually have carinae and distally-recurved crowns which are ideal for eating prey-items larger than the gullet by cutting prey into consumable pieces. These recurved teeth potentially aid in processing prey; the Australian fur seal (*Arctocephalus pusillus doriferus*) and the leopard seal (*Hydrurga leptonyx*) possess recurved canines that help these predators to grip prey, which they then shake against the water surface [50,51]. The pterygoid teeth of mosasaurids might have also been adapted for gripping, although to serve in the intraoral transport of prey [52], and are absent in durophagous taxa such as *Globidens*. Small-prey flesh eaters generally have small, conical teeth with a high aspect ratio (2 to 3 times high as wide) which are well suited for dispatching small soft-bodied teleosts and coleoids or, if relatively long and procumbent, can be used as a trapping device as in some long-necked plesiosaurians [53].

Even if our high-density sampling protocol is able to capture dental ornamentation such as ridges and carinae (Fig. S2), the presence or absence of such structures will result in minor displacement of some surface semi-landmarks in the three-dimensional space. In turn, because they do not account for much of crown shape variation across our entire sample, these structures will thus not be captured by the first axes of a PCA despite having a functional signal [54]. This is a limitation of our method when applied to datasets with large shape variation such as this one and we recommend systematically pairing quantitative palaeobiological analyses with thorough, first-hand anatomical data when discussing finer patterns of niche partitioning, such as in Foffa et al. [13].

(c) Convergence and constraints

The very high density of morphospace occupation on slightly negative values on PC1 and our OPCR analyses powerfully illustrate the strength of a long-known phenomenon in aquatic amniotes: convergent dental simplification [6,55]. This phenomenon transcends size and species-relatedness (Figs. 2, 3, S6), and canalised the dental evolution of most raptorial marine amniotes towards simple conical teeth.

Yet, many Cenozoic taxa fall within the morphospace and guilds previously evolved by Mesozoic marine reptiles (Figs. 2, S7) and their maximal occupation densities are close as well (Fig. S7), indicating convergent evolution of an array of (fairly simple) shapes, which we show are related to diet. In addition to convergent simplification [55] and convergent evolution of crown shapes [6,54], the patterns of morphospace occupation are also driven by the existence of wide unoccupied regions, which can notably be explained in a functional framework. For example, strong labiolingual flattening (high positive values on PC2) combined with a narrow cross-section and strong curvature (negative values on PC1) would make the teeth unable to resist sufficient apicobasal stress to function in prey capture or mastication. Similarly, the region in between clear durophages like placodonts and globidensine mosasaurids and 'conical' toothed taxa is sparsely occupied only by a couple of gigantic taxa (*Prognathodon currii*, *Livyatan melvillei*, and likely *Machimosaurus*, which we did not analyse). This suggests that these intermediate morphologies (i.e. high domes) are possibly suboptimal for either crushing or piercing prey items, as shelled sea food is often protected by a thick mineralised armour since the Mesozoic marine revolution [56]. These tooth morphologies are, however, frequent in small, arthropod-eating terrestrial squamates [35] (see also ref [57]). With that said, it is also important to note that factors beyond functional constraints could influence the patterns of morphospace occupation observed in our results. Teeth can develop into an amazing array of shapes, but conical teeth are still limited in form by developmental constraints that prevent certain extreme areas of morphospace being occupied [58]. Similarly, other factors such as phylogenetic inertia could drive patterns observed in the results. Nevertheless, our new data on the ecological signal in the shape and size of marine amniote teeth combines with the existence of unique Mesozoic morphologies, such as carinated, trihedral, and 'trapping' teeth (Figs. 2, S7 [53]), in illustrating how macroecological changes in ecosystems [59] shape their predators over hundreds of millions of years.

ACKNOWLEDGMENTS AND FUNDING SOURCES

A long series of curators, colleagues, and data handlers have made this study possible by loaning specimens and providing 3D models. We warmly thank them collectively here (a detailed list can be found in the supplementary information). We also thank the two anonymous colleagues who reviewed this paper, providing a series of thoughtful and constructive suggestions! The present version of the paper also benefited from interesting discussions held during the 9th SECAD meeting in Chile, notably with Dr. Judith Pardo-Pérez and Prof. Judy Massare. We benefited from funding from the Fonds pour la Recherche Scientifique FNRS (MIS F.4511.19 grant [V.F., J.A.M.], a FRIA fellowship FC 23645 [R.F.B.]), and a PHC Tournesol grant (V.F., N.B.).

REFERENCES

1. Vermeij GJ, Motani R. 2018 Land to sea transitions in vertebrates: the dynamics of colonization. *Paleobiology* **44**, 237–250. (doi:10.1017/pab.2017.37)
2. Bardet N, Falconnet J, Fischer V, Houssaye A, Jouve S, Pereda-Suberbiola X, Pérez-García A, Rage J-CJ-C, Vincent P. 2014 Mesozoic marine reptile palaeobiogeography in response to drifting plates. *Gondwana Research* **26**, 869–887. (doi:10.1016/j.gr.2014.05.005)
3. Lindgren J, Polcyn MJ, Young BA. 2011 Landlubbers to leviathans: evolution of swimming in mosasaurine mosasaurs. *Paleobiology* **37**, 445–469.
4. Bernard A *et al.* 2010 Regulation of body temperature by some Mesozoic marine reptiles. *Science (1979)* **328**, 1379–1382.
5. Houssaye A. 2013 Bone histology of aquatic reptiles: what does it tell us about secondary adaptation to an aquatic life? *Biological Journal of the Linnean Society* **108**, 3–21. (doi:10.1111/j.1095-8312.2012.02002.x)
6. Massare JA. 1987 Tooth morphology and prey preference of Mesozoic marine reptiles. *Journal of Vertebrate Paleontology* **7**, 121–137.
7. Kelley NP, Motani R. 2015 Trophic convergence drives morphological convergence in marine tetrapods. *Biology Letters* **11**, 1–5.
8. Ciampaglio CN, Wray GA, Corliss BH. 2005 A toothy tale of evolution: convergence in tooth morphology among Marine Mesozoic - Cenozoic sharks, reptiles, and mammals. *The Sedimentary Record* **3**, 4–8.
9. Bardet N, Houssaye A, Vincent P, Pereda X, Amaghzaz M, Jourani E, Meslouh S. 2015 Mosasaurids (Squamata) from the Maastrichtian Phosphates of Morocco: Biodiversity , palaeobiogeography and palaeoecology based on tooth morphoguilds. *Gondwana Research* **27**, 1068–1078. (doi:10.1016/j.gr.2014.08.014)
10. Ridgway SH, Harrison R. 1999 *The Second Book of Dolphins and the Porpoise*. San Diego: Academic Press.
11. Benson RBJ, Evans M, Smith AS, Sassoon J, Moore-Faye S, Ketchum HF, Forrest R. 2013 A giant pliosaurid skull from the Late Jurassic of England. *PLoS ONE* **8**, e65989. (doi:10.1371/journal.pone.0065989)
12. Zverkov NG, Fischer V, Madzia D, Benson RBJ. 2018 Increased Pliosaurid Dental Disparity Across the Jurassic – Cretaceous Transition. *Palaeontology* **61**, 825–846. (doi:10.1111/pala.12367)
13. Foffa D, Young MT, Stubbs TL, Dexter KG, Brusatte SL. 2018 The long-term ecology and evolution of marine reptiles in a Jurassic seaway. *Nature Ecology and Evolution* **2**, 1548–1555. (doi:10.1038/s41559-018-0656-6)
14. Madzia D, Sachs S, Young M, Lukeneder A, Skupien P. 2021 Evidence of two lineages of metriorhynchid crocodylomorphs in the Lower Cretaceous of the Czech Republic. *Acta Palaeontologica Polonica* **66**. (doi:10.4202/app.00801.2020)
15. Bardet N, Falconnet J. 2014 Niche partioning using tooth morphoguilds in mosasaurid faunas from the Maastrichtian Phosphates of Morocco: a

quantitative approach. In *74th Annual Meeting of the Society of Vertebrate Paleontology*, p. 85. Berlin, Germany.
16. Goswami A, Watanabe A, Felice RN, Bardua C, Fabre AC, Polly PD. 2019 High-Density Morphometric Analysis of Shape and Integration: The Good, the Bad, and the Not-Really-a-Problem. *Integrative and Comparative Biology* **59**, 669–683. (doi:10.1093/icb/icz120)
17. Bardua C, Felice RN, Watanabe A, Fabre A, Goswami A. 2019 A Practical Guide to Sliding and Surface Semilandmarks in Morphometric Analyses. *Integrative Organismal Biology* , 1–34. (doi:10.1093/iob/obz016)
18. Cardini A. 2020 Less tautology, more biology? A comment on “high-density” morphometrics. *Zoomorphology* **139**, 513–529. (doi:10.1007/s00435-020-00499-w)
19. Boyer DM, Lipman Y, st. Clair E, Puente J, Patel BA, Funkhouser T, Jernvall J, Daubechies I. 2011 Algorithms to automatically quantify the geometric similarity of anatomical surfaces. *Proceedings of the National Academy of Sciences* **108**, 18221–18226. (doi:10.1073/pnas.1112822108)
20. Konishi T, Brinkman DB, Massare JA, Caldwell MW. 2011 New exceptional specimens of Prognathodon overtoni (Squamata, Mosasauridae) from the upper Campanian of Alberta, Canada, and the systematics and ecology of the genus. *Journal of Vertebrate Paleontology* **31**, 1026–1046. (doi:10.1080/02724634.2011.601714)
21. Bianucci G, Geisler JH, Citron S, Collareta A. 2022 The origins of the killer whale ecomorph. *Current Biology* **32**, 1843-1851.e2. (doi:10.1016/j.cub.2022.02.041)
22. Christensen K, Melstrom KM. 2021 Quantitative analyses of squamate dentition demonstrate novel morphological patterns. *PLoS ONE* **16**, 1–16. (doi:10.1371/journal.pone.0257427)
23. Cignoni P, Callieri M, Corsini M, Dellepiane M, Ganovelli F, Ranzuglia G. 2008 MeshLab: an Open-Source Mesh Processing Tool. In *Eurographics Italian Chapter Conference* (eds V Scarano, R de Chiara, U Erra), The Eurographics Association. (doi:10.2312/LocalChapterEvents/ItalChap/ItalianChapConf2008/129-136)
24. Konishi T, Newbrey MG, Caldwell MW. 2014 A small, exquisitely preserved specimen of Mosasaurus missouriensis (Squamata, Mosasauridae) from the upper Campanian of the Bearpaw Formation, western Canada, and the first stomach contents for the genus. *Journal of Vertebrate Paleontology* **34**, 802–819. (doi:10.1080/02724634.2014.838573)
25. Boyer DM, Puente J, Gladman JT, Glynn C, Mukherjee S, Yapuncich GS, Daubechies I. 2015 A New Fully Automated Approach for Aligning and Comparing Shapes. *Anatomical Record* **298**, 249–276. (doi:10.1002/ar.23084)
26. R Core Team. 2016 R: A language and environment for statistical computing.
27. Adams D, Collyer M, Kaliontzopoulou A. 2020 Geomorph: Software for geometric morphometric analyses.
28. Schlager S, Jefferis G, Dryden I. 2021 Morpho: calculations and visualisations related to geometric morphometrics.

29. Fischer V, Maclaren JA, Soul LC, Bennion RF, Druckenmiller PS, Benson RBJ. 2020 The macroevolutionary landscape of short-necked plesiosaurians. *Sci Rep* **10**, 1–12. (doi:10.1038/s41598-020-73413-5)
30. Madzia D, Cau A. 2020 Estimating the evolutionary rates in mosasauroids and plesiosaurs : discussion of niche occupation in Late Cretaceous seas. *Peer* **8**, 1–31. (doi:10.7717/peerj.8941)
31. Pampush JD, Winchester JM, Morse PE, Vining AQ, Boyer DM, Kay RF. 2016 Introducing molaR: a New R Package for Quantitative Topographic Analysis of Teeth (and Other Topographic Surfaces). *Journal of Mammalian Evolution* **23**, 397–412. (doi:10.1007/s10914-016-9326-0)
32. Melstrom KM, Angielczyk KD, Ritterbush KA, Irmis RB. 2021 The limits of convergence: the roles of phylogeny and dietary ecology in shaping non-avian amniote crania. *Royal Society Open Science* **8**, 202145. (doi:10.1098/rsos.202145)
33. Lambert O, Bianucci G, Post K, de Muizon C, Salas-Gismondi R, Urbina M, Reumer J. 2010 The giant bite of a new raptorial sperm whale from the Miocene epoch of Peru. *Nature* **466**, 105–108.
34. Sassoon J, Foffa D, Marek R. 2015 Dental ontogeny and replacement in Pliosauridae. *Royal Society Open Science* **2**, 150384. (doi:10.1098/rsos.150384)
35. Melstrom KM. 2017 The relationship between diet and tooth complexity in living dentigerous saurians. *Journal of Morphology* **278**, 500–522. (doi:10.1002/jmor.20645)
36. Massare JA. 1997 Faunas, behavior, and evolution. In *Ancient Marine Reptiles* (eds JM Callaway, EL Nicholls), pp. 401–421. San Diego: Academic Press.
37. Buchy M-C. 2010 Morphologie dentaire et régime alimentaire des reptiles marins du Mésozoïque : revue critique et réévaluation. *Oryctos* **9**, 49–82.
38. Werth AJ. 2005 Functional Morphology of the Sperm Whale (Physeter macrocephalus) Tongue, with Reference to Suction Feeding. *Aquatic Mammals* **30**, 405–418. (doi:10.1578/am.30.3.2004.405)
39. Nilsson D-E, Warrant EJ, Johnson S, Hanlon R, Shashar N. 2012 A unique advantage for giant eyes in giant squid. *Current Biology* **22**, 683–688. (doi:10.1016/j.cub.2012.02.031)
40. Noe LF. 1999 The Callovian pliosaurs of the Oxford Clay–evidence and implications for the consumption of marine invertebrates. In *Secondary Adaptation to Life in Water/La réadaptation au milieu aquatique*, pp. 13–17.
41. Cohen KE, Weller HI, Westneat MW, Summers AP. 2020 The Evolutionary Continuum of Functional Homodonty to Heterodonty in the Dentition of *Halichoeres* Wrasses. *Integrative and Comparative Biology* , 1–12. (doi:10.1093/icb/icaa137)
42. Huene F von. 1922 *Die Ichthyosaurier des Lias und ihre Zusammenhänge*. Berlin: Verlag von Gebrüder Borntraeger.

43. McGowan C. 1973 The cranial morphology of the Lower Liassic latipinnate ichthyosaurs of England. *Bulletin of the British Museum (Natural History) Geology* **24**, 1–109.
44. Lomax DR. 2010 An *Ichthyosaurus* (Reptilia, Ichthyosauria) with gastric contents from Charmouth, England: first report of the genus from the Pliensbachian. *Paludicola* **8**, 22–36.
45. Böttcher VR. 1989 Über die Nahrung eines *Leptopterygius* (Ichthyosauria, Reptilia) aus dem süddeutschen Posidonienschiefer (Unterer Jura) mit Bemerkungen über den Magen der Ichthyosaurier. *Stuttgarder Beiträge zur Naturkunde Serie B (Geologie und paläontologie)* **155**, 1–19.
46. Ford JKB, Ellis GM, Matkin CO, Wetklo MH, Barrett-Lennard LG, Withler RE. 2011 Shark predation and tooth wear in a population of northeastern pacific killer whales. *Aquatic Biology* **11**, 213–224. (doi:10.3354/ab00307)
47. Eschricht DF. 1866 On the species of the genus Orca inhabiting the northern seas. In *Recent memoires on the Cetacea*, pp. 153–188.
48. Motani R. 2002 Scaling effects in caudal fin propulsion and the speed of ichthyosaurs. *Nature* **415**, 309–312.
49. Fischer V, Arkhangelsky MS, Stenshin IM, Uspensky GN, Zverkov NG, Benson RBJ. 2015 Peculiar macrophagous adaptations in a new Cretaceous pliosaurid. *Royal Society Open Science* **2**, 150552. (doi:10.1098/rsos.150552)
50. Hocking DP, Fitzgerald EMG, Salverson M, Evans AR. 2016 Prey capture and processing behaviors vary with prey size and shape in Australian and subantarctic fur seals. *Mar Mamm Sci* **32**, 568–587. (doi:10.1111/mms.12285)
51. Robbins JR, Poncet D, Evans AR, Hocking DP. 2019 A rare observation of group prey processing in wild leopard seals (Hydrurga leptonyx). *Polar Biology* **42**, 1625–1630. (doi:10.1007/s00300-019-02542-z)
52. Russell AP. 1967 Systematics and morphology of American mosasaurs (Reptilia, Sauria). *Peabody Museum of Natural History of the Yale University* **23**, 1–240.
53. Chatterjee S, Small BJ. 1989 New plesiosaurs from the Upper Cretaceous of Antarctica. *Geological Society, London, Special Publications* **47**, 197–215. (doi:10.1144/GSL.SP.1989.047.01.15)
54. McCurry MR, Evans AR, Fitzgerald EMG, McHenry CR, Bevitt J, Pyenson ND. 2019 The repeated evolution of dental apicobasal ridges in aquatic-feeding mammals and reptiles. *Biological Journal of the Linnean Society* , In press. (doi:10.1093/biolinnean/blz025)
55. Peredo CM, Peredo JS, Pyenson ND. 2018 Convergence on dental simplification in the evolution of whales. *Paleobiology* **44**, 434–443. (doi:10.1017/pab.2018.9)
56. Vermeij GJ. 2015 The Mesozoic marine revolution: evidence from snails, predators and grazers. *Paleobiology* **3**, 245–258.
57. Schulp AS. 2005 Feeding the mechanical mosasaur: What did *Carinodens* eat? *Geologie en Mijnbouw/Netherlands Journal of Geosciences* **84**, 345–357. (doi:10.1017/S0016774600021132)

58. Evans AR *et al.* 2021 A universal power law for modelling the growth and form of teeth, claws, horns, thorns, beaks, and shells. *BMC Biology* **19**, 1–14. (doi:10.1186/s12915-021-00990-w)
59. Bambach RK. 1993 Seafood through time. *Paleobiology* **19**, 372–397.

SUPPLEMENTARY INFORMATION

Ecological signal in the size and shape of marine amniote teeth

Valentin Fischer[1,*], Rebecca F. Bennion[1,2], Davide Foffa[3,4,5], Jamie A. MacLaren[1,6], Matthew R. McCurry[7,8,9], Keegan M. Melstrom[10,11], Nathalie Bardet[12]

[1] Evolution & Diversity Dynamics Lab, Université de Liège, 4000 Liège, Belgium.
[2] Palaeobiosphere evolution, Royal Belgian Institute of Natural Sciences, Brussels Belgium.
[3] Department of Natural Sciences, National Museums Scotland, Edinburgh EH1 1JF, United Kingdom
[4] School of Geography, Earth and Environmental Sciences, University of Birmingham, Birmingham B15 2TT, United Kingdom
[5] Department of Geosciences, Virginia Tech, Blacksburg, Virginia 24061, USA
[6] Functional Morphology Lab, Department of Biology, Universiteit Antwerpen, 2610 Antwerpen, Belgium
[7] Australian Museum Research Institute, Sydney, New South Wales 2010, Australia.
[8] Earth and Sustainability Science Research Centre, School of Biological, Earth and Environmental Sciences (BEES), University of New South Wales, Kensington, New South Wales 2052, Australia.
[9] Paleobiology, National Museum of Natural History, Smithsonian Institution, Washington, DC 20560, USA.
[10] Engineering and Science Division, Rose State College, Midwest City, OK 73110, USA
[11] Dinosaur Institute, Natural History Museum of Los Angeles County, Los Angeles, CA, 90007 USA
[12] CR2P, Muséum National d'Histoire Naturelle, 75005 Paris, France

* corresponding author: Valentin Fischer, v.fischer@uliege.be

DOI: 10.1098/rspb.2022.1214

SUPPLEMENTARY TABLES

Table S1. Metadata of each specimen used in this study. Region of origin specifies the anatomical region where the crown was extracted, if known, and also indicates alteration made to the model (mirroring, crack removal, etc.). Institutional abbreviations: BHN: Musée Boulogne-sur-Mer, France; BRLSI: Bath Royal Literary & Scien- tific Institution, Bath, UK; CAMSM: Sedgwick Museum of Earth Sciences, University of Cambridge, Cambridge, UK; CCNHM: Mace Brown Museum College of Charleston, Charleston, South Carolina, USA ; FCG: Fundación Colombiana de Geobiología, Bogotá, Colombia; FHSM: ort Hays State University Sternberg Museum of Natural History, Hays, Kansas, USA; IRSNB: Institut Royal des Sciences Naturelles de Belgique, Brussels, Belgium; KK: Kronosaurus Korner, Richmond, Australia; KUVP: University of Kansas Natural History Museum, Lawrence, Kansas, USA; MCZR: Monash University Zoological Research Collections, Clayon, Australia ; MNHN: Muséum National d'Histoire Naturelle, Paris, France; MNHNL: Muséum national d'histoire naturelle du Luxembourg, Luxembourg-ville, Luxembourg; MUSM: Museo de Historia Natural, Universidad Nacional Mayor de San Marcos, Lima, Peru ; NMML: Port Townsend Marine Science Center, Washington, USA; OCP: Office Chérifien des Phosphates, Khouribga, Morocco; PIMUZ: Paläontologisches Institut und Museum, Zürich, Switzerland; QM: Queensland Museum, Brisbane, Australia ; SMNS: Staatliches Museum für Naturkunde Stuttgart, Germany; UF: Florida Museum of Natural History, Gainesville, USA ; ULgPA: Université de Liège, collections de paléontologie, Liège, Belgium; USNM: United States National Museum of Natural History, Smithsonian Institution, Washington DC, USA .

Taxon	Clade	Specimen	Source	Region of origin
Brachauchenius lucasi	Sauropterygia	FHSM VP-17957	Photogrammetry (FHSM)	NA
Carinodens belgicus	Mosasauroidea	MNHN6338 (cast)	Photogrammetry (Pierre Sparla)	right maxilla or left dentary, mirrored
Cf. Nannopterygius	Ichthyosauria	CAMSM TN3753.1	Laser, 0.2mm precision	right maxilla or left dentary, mirrored
Cf. Zarafasaura	Sauropterygia	OCP667	Laser, 0.2mm precision	NA
Clidastes propython	Mosasauroidea	FHSM VP17576	Laser, 0.2mm precision	right maxilla or left dentary, mirrored

Cyamodus kuhnschnyderi	Sauropterygia	SMNS 15855	CT-scan (Torsten Scheyer)	right maxilla, mirrored, anterior tooth
Cynthiacetus peruvianus	Cetacea	MNHN.F.PRU10	Laser, 0.2mm precision	right dentary
Dakosaurus sp.	Archosauromorpha	CAMSM J29449	Laser, 0.2mm precision, small crack removed	NA
Delphinus delphis	Cetacea	MCZR10088	CT-scan (Ref [1], on Morphosource)	right dentary
Dolichorhynchops bonneri	Sauropterygia	KUVP40001	Laser, 0.2mm precision (Ref [2], on Morphosource)	right pmx
Ectenosaurus clidastoides	Mosasauroidea	FHSM 401	Laser, 0.2mm precision	right maxilla, mirrored
Eosqualodon sp. nov.	Cetacea	CCNHM 170.1	Laser (Ellen Coombs & Morgan Churchill)	left maxilla
Eurhinosaurus longirostris	Ichthyosauria	MNHNL TU112	Laser, 0.2mm precision	NA
Feresa attenuata	Cetacea	USNM 504917	Laser, 0.2mm precision	right dentary
Gaviali gangeticus	Archosauromorpha	UF Herp 118998	CT-scan (Blackburn lab on Morphsource)	left dentary, mirrored
Geosaurinae indet.	Archosauromorpha	CAMSM TN3753.2	Laser, 0.2mm precision	NA
Globidens dakotensis	Mosasauroidea	FHSM VP13828	Laser, 0.2mm precision	right maxilla or left dentary, mirrored, anterior tooth
Globidens dakotensis	Mosasauroidea	FHSM VP13828	Laser, 0.2mm precision	right maxilla or left dentary, mirrored, anterior tooth
Globidens phosphaticus	Mosasauroidea	ULgPA20220411-1	Photogrammetry (Pierre Sparla)	NA, posterior tooth
Kronosaurus queenslandicus	Sauropterygia	KKF0534	CT-scan (Ref [3])	NA
Lemmysuchus obtusidens	Archosauromorpha	CAMSM J.65408	Photogrammetry	NA

Liopleurodon ferox	Sauropterygia	Cast of BHN 3R 197	Laser, 0.2mm precision	right maxilla or left dentary, mirrored
Livyatan melvilei	Cetacea	MUSM 1676	Laser; Ref [4] for skull measurements	dentary 3
Megacephalosaurus eulerti	Sauropterygia	FHSM VP-321	White-light (Chase Shelburne; see also Ref [2], on Morphosource)	left dentary, mirrored
Microcleidus melusinae	Sauropterygia	MNHNLTV434	Laser, 0.2mm precision	left maxilla
Mosasaurus hoffmanni	Mosasauroidea	ULgPa25119a	Laser, 0.2mm precision	right maxilla or left dentary, mirrored
Mosasaurus lemmonieri	Mosasauroidea	IRSNB R366	Laser, 0.2mm precision	right maxilla or left dentary, mirrored
Muiscasaurus catheti	Ichthyosauria	FCG-CBP-16	Photogrammetry (Ref [5]); scaled manually	NA
Muraenosaurus leedsi	Sauropterygia	CAMSM TN3753.3	Laser, 0.2mm precision; ca. 1.5mm of tip reconstructed	NA
Ninoziphius platyrostris	Cetacea	USNM 526533	CT-scan (Ref [6])	NA
Orcinus orca	Cetacea	NMML-1850_M12791-21528	Laser (Idaho Virtualization Lab on Morphosource)	right dentary
Orcinus orca	Cetacea	USNM 241401	CT-scan (Ref [6])	NA, worn tooth
Pelagosaurus typus	Archosauromorpha	BRLSI M1413	CT-scan (Ref [7]); slight reconstruction	right dentary
Placodus gigas	Sauropterygia	OMU BT13	CT-scan (Torsten Scheyer)	left maxilla
Platecarpus tympaniticus	Mosasauroidea	KUVP 1007	Laser, 0.2mm precision	right maxilla or left dentary, mirrored
Platypterygius australis	Ichthyosauria	QMF551	Laser, 0.2mm precision	NA
Platypterygius sp.	Ichthyosauria	CAMSM TN1716.15	Laser, 0.2mm precision	right maxilla or left

				dentary, mirrored
Pliosaurus grossouvrei	Sauropterygia	CAMSMJ13304	Laser, precision 0.2mm	right maxilla or left dentary, mirrored
Pliosaurus sp. (round)	Sauropterygia	CAMSM J60897	Laser, precision 0.2mm	right maxilla or left dentary, mirrored
Pliosaurus sp. (subtrihedral)	Sauropterygia	CAMSM J29552	Laser, precision 0.2mm	right maxilla or left dentary, mirrored
Pliosaurus sp. (trihedral)	Sauropterygia	CAMSM J29544	Laser, precision 0.2mm	NA
Pliosaurus sp.	Sauropterygia	CAMSM J29554	Laser, precision 0.2mm	NA, worn tooth
Polyptychodon interruptus	Sauropterygia	CAMSM 57378	Laser, precision 0.2mm	NA
Pontoporia blainvillei	Cetacea	IRSNB1506	Laser, precision 0.3mm	right dentary
Prognathodon currii	Mosasauroidea	ULgPA20220209-1	Laser, precision 0.2mm	NA, sediment removed
Prognathodon solvayi	Mosasauroidea	IRSNB R33b	Laser, precision 0.2mm	NA, small damage removed
Psephoderma alpinum	Sauropterygia	PIMUZ A III 1491	CT-scan (Torsten Scheyer)	left maxilla, anterior tooth
Selmasaurus johnsoni	Mosasauroidea	FHSM VP13910	Laser, precision 0.2mm	left maxilla
Sisteronia seeleyi	Ichthyosauria	CAMSM TN1779.1.10	Laser, precision 0.2mm	left dentary, mirrored
Steno bredanensis	Cetacea	IRSNB 1515y	Laser, precision 0.4mm	left maxilla
Tanystropheus hydroides	Archosauromorpha	PIMUZ T 2790	CT-scan (Ref [8]); scaled manually	right maxilla, mirrored, glitch removed
Teleosauroidae indet.	Archosauromorpha	CAMSM J29458	Laser, precision 0.2mm	right maxilla or left dentary, mirrored

Temnodontosaurus platyodon	Ichthyosauria	IRSNB R122	Laser, precision	0.2mm	NA
Thalattosuchus superciliosus	Archosauromorpha	CAMSM J65414	Laser, precision	0.2mm	NA
Tylosaurus bernardi	Mosasauroidea	IRSNB 23A	Laser, precision	0.2mm	right dentary
Tylosaurus cf. nepaeolicus	Mosasauroidea	FHSM VP13733	Laser, precision	0.2mm	left dentary, mirrored
Tyrannoneustes lythrodectikos	Archosauromorpha	CAMSM 64373	Laser, precision	0.2mm	right maxilla or left dentary, mirrored

Table S2. Metadata of the supplementary specimens onto which our protocol has been applied. "Region of origin" specifies the anatomical region where the crown was extracted, if known, as well as alterations made to the model (mirroring, crack removal, etc.), if any. Additional institutional abbreviations: BIRUG: Lapworth Museum, University of Birmingham, UK; LACM: Natural History Museum of Los Angeles County, Los Angeles, CA, USA.

Taxon	Clade	Specimen	Source	Region of origin
Iguanodon bernissartensis	Archosauromorpha	IRSNB R1534	White light, 0.5 mm precision	Left manus
Cyamodus kuhnschnyderi	Sauropterygia	SMNS 15855	CT-scan (Torsten Scheyer)	right maxilla, mirrored
Hibolites sp.	Belemnitoidea	NA, Université Aix-Marseille	Photogrammetry (Université Aix-Marseille on Sketchfab)	NA
Otodus megalodon	Chondrichtyes	BIRUG 14906	Photogrammetry (?) (Lapworth Museum on Sketchfab)	NA
Smilodon fatalis	Mammalia	LACM HC 2001-2	Laser, 0.2mm precision	right maxilla, mirrored

Table S3. Dietary categories based on gut content.

Dietary category	Diet
Flesh, large	can contain large vertebrates (soft exterior, harder interior)
Flesh, medium	composed of medium-sized prey items (body < 20cm) with hard interior (medium-sized vertebrates such as many birds, coleoid cephalopods)
Flesh, small	solely consists of small and soft animals (small vertebrates, squids).
Shelled, large	composed of large shelled animals (hard exterior, soft interior; vertebrates and invertebrates such as turtles and large ammonites)
Shelled, small	composed of small shelled animals (hard exterior, soft interior; essentially benthic invertebrates such as echinoderms, bivalves, and gastropods)

Table S4. Guild, size, dietary, and OPCR data for each specimen. All specimens are from the Mesozoic, except all cetaceans and Gavialis gangeticus. These data are also provided as a machine-readable .csv file as supplementary information.

File_ID	Mass are	Gastric_content	Mandible_length	Interglenoid_dist	OPCR_3	OPCR_5
Brachauchenius_lucasi	General	NA	NA	NA	8.25	8
Carinodens_belgicus	Crush	Shell_large	NA	NA	8.875	8.75
Cf_Nannopterygius	Pierce	NA	NA	NA	8.25	8.125
Cf_Tylosaurus_nepaeolicus	Cut	Flesh_large	NA	NA	8.375	8.125
Cf_Zarafasaura	Pierce	NA	NA	NA	8.62	8.25
Clidastes_propython	General	NA	359	72	8.75	8.25
Cyamodus_kuhnschnyderi_ant	Crush	NA	191	123	9.75	9.125
Cynthiacetus_peruvianus	General	NA	1018	224	8	8
Dakosaurus_sp	Cut	NA	NA	NA	10.5	8.75
Delphinus_delphis	Pierce	Flesh_small	NA	NA	8.38	8.12
Dolichorhynchops_bonneri	Pierce	NA	968	224	9.5	8.5
Ectenosaurus_clidastoides	Cut	NA	642	170	8.12	8.12
Eosqualodon_nsp	Cut	NA	681	232	9	8.5
Eurhinosaurus_longirostris	Pierce	NA	NA	NA	8.5	8
Feresa_attenuata	Pierce	Flesh_med	279	153	8	8
Gavialis_gangeticus	Pierce	Flesh_small	604	127	9.88	8.5
Geosaurine_indet	Cut	NA	NA	NA	8	8

Globidens_dakotensis_ant	Crush	Shell_small	NA	212	10.88	9.88
Globidens_dakotensis_post	Crush	Shell_small	NA	212	8	8
Globidens_phosphaticus_post	Crush	Shell_small	NA	NA	8.25	8
Kronosaurus_queenslandicus	Pierce	NA	NA	NA	23.75	12.38
Lemmysuchus_obtusidens	Crunch	NA	NA	NA	8.12	8
Liopleurodon_ferox	Pierce	NA	NA	NA	8.62	8.25
Livyatan_melvilei	Crunch	NA	3000	1900	19.38	13
Megacephalosaurus_eulerti	Pierce	NA	1714	NA	8.62	8.38
Microcleidus_melusinae	Pierce	NA	183	57	8.75	8.5
Mosasaurus_hoffmanni	Cut	Flesh_large	NA	NA	10.75	9.38
Mosasaurus_lemmonieri	Pierce	Flesh_large	870	NA	8	8
Muiscasaurus_catheti	Pierce	NA	742	NA	8.12	8
Muraenosaurus_leedsi	Pierce	NA	NA	NA	8.5	8.25
Ninoziphius_platyrostris	Smash	NA	NA	NA	9.62	8.88
Orcinus_orca	Smash	Flesh_large	823	361	8.75	8.75
Orcinus_orca_worn	Smash	Flesh_large	NA	NA	8.12	8
Pelagosaurus_typus	Pierce	Flesh_small	286	28	12	11.38
Placodus_gigas_ant	Crush	NA	185	67	8.75	8.5
Platecarpus_tympanitic us	Cut	Flesh_large, Shell_large	612	188	8.88	8.12
Platypterygius_australis	Pierce	Flesh_large	1136	253	8.12	8.12
Platypterygius_sp	Smash	Flesh_large	NA	NA	8	8
Pliosaurus_grossouvrei	General	NA	NA	NA	8.375	8.25
Pliosaurus_round	General	NA	NA	NA	9.375	8.375
Pliosaurus_subtrihedral	General	NA	NA	NA	9.625	9
Pliosaurus_trihedral	Cut	NA	NA	NA	11.625	10.875
Pliosaurus_worn	General	NA	NA	NA	8.125	8
Polyptychodon_interruptus	General	NA	NA	NA	8.75	8
Pontoporia_blainvillei	Pierce	Flesh_small	301	84	8.5	8

Prognathodon_currii	Crunch	NA	NA	NA	8.88	8.75
Prognathodon_solvayi	Cut	NA	606	187	9.5	9.38
Psephoderma_alpinum_ant	Crush	NA	117	53	12.75	11.5
Selmasaurus_johnsoni	Cut	NA	386	91	9.38	9.25
Sisteronia_seeleyi	Pierce	NA	NA	NA	8	8
Steno_bredanensis	General	Flesh_small	462	118	8.38	8
Tanystropheus_hydroides	Pierce	NA	129	34	9.88	8.75
Teleosauroid_indet	Cut	NA	NA	NA	8.12	8
Temnodontosaurus_platyodon	Cut	Flesh_large	NA	NA	12.88	10
Thalattosuchus_superciliosus	Cut	NA	NA	NA	8	8
Tylosaurus_bernardi	Cut	Flesh_large, Flesh_med	1516	392	13.5	11.5
Tyrannoneustes_lythrodectikos	Pierce	NA	NA	NA	8.75	8.5

Table S5. Eigenvalues and proportion of variance of each axis resulting from the PCA.

	Comp1	Comp2	Comp3	Comp4	Comp5	Comp6	Comp7	Comp8	Comp9	Comp10
Eigenvalues	0.05982599	0.00280135	0.00191026	0.00112087	0.00063039	0.00043977	0.00041462	0.00037564	0.00021818	0.0001545
Proportion of variance	0.86725147	0.04060901	0.02769155	0.01624835	0.00913826	0.00637501	0.00601035	0.0054454	0.00316275	0.00223969
Cumulative proportion	0.86725147	0.90786048	0.93555203	0.95180039	0.96093864	0.96731366	0.97332401	0.97876941	0.98193216	0.98417185
	Comp11	Comp12	Comp13	Comp14	Comp15	Comp16	Comp17	Comp18	Comp19	Comp20
Eigenvalues	0.00013604	0.00011556	0.00010692	9.85E-05	8.75E-05	7.45E-05	5.99E-05	4.97E-05	3.96E-05	3.46E-05
Proportion of variance	0.00197203	0.00167523	0.00154989	1.43E-03	1.27E-03	1.08E-03	8.68E-04	7.21E-04	5.74E-04	5.01E-04
Cumulative proportion	0.98614388	0.98781912	0.989369	9.91E-01	9.92E-01	9.93E-01	9.94E-01	9.95E-01	9.95E-01	9.96E-01
	Comp21	Comp22	Comp23	Comp24	Comp25	Comp26	Comp27	Comp28	Comp29	Comp30
Eigenvalues	2.79E-05	2.63E-05	2.44E-05	2.34E-05	1.82E-05	1.75E-05	1.48E-05	1.39E-05	1.18E-05	1.14E-05
Proportion of variance	4.04E-04	3.82E-04	3.54E-04	3.39E-04	2.64E-04	2.54E-04	2.14E-04	2.01E-04	1.71E-04	1.66E-04
Cumulative proportion	9.96E-01	9.97E-01	9.97E-01	9.97E-01	9.98E-01	9.98E-01	9.98E-01	9.98E-01	9.98E-01	9.99E-01
	Comp31	Comp32	Comp33	Comp34	Comp35	Comp36	Comp37	Comp38	Comp39	Comp40
Eigenvalues	9.54E-06	8.36E-06	8.21E-06	7.90E-06	6.49E-06	5.80E-06	5.36E-06	5.16E-06	4.58E-06	4.06E-06
Proportion of variance	1.38E-04	1.21E-04	1.19E-04	1.15E-04	9.40E-05	8.41E-05	7.77E-05	7.47E-05	6.64E-05	5.88E-05
Cumulative proportion	9.99E-01	9.99E-01	9.99E-01	9.99E-01	9.99E-01	9.99E-01	9.99E-01	9.99E-01	9.99E-01	1.00E+00
	Comp41	Comp42	Comp43	Comp44	Comp45	Comp46	Comp47	Comp48	Comp49	Comp50

Eigenvalues	3.62E-06	3.52E-06	3.39E-06	3.05E-06	2.86E-06	2.51E-06	2.38E-06	2.16E-06	1.88E-06	1.79E-06
Proportion of variance	5.24E-05	5.10E-05	4.91E-05	4.42E-05	4.14E-05	3.63E-05	3.46E-05	3.13E-05	2.72E-05	2.60E-05
Cumulative proportion	1.00E+00	1.00E+00	1.00E+00	1.00E+00	1.00E+00	1.00E+00	1.00E+00	1.00E+00	1.00E+00	1.00E+00
	Comp51	Comp52	Comp53	Comp54	Comp55	Comp56				
Eigenvalues	1.41E-06	1.24E-06	1.20E-06	1.02E-06	9.63E-07	9.01E-07				
Proportion of variance	2.04E-05	1.80E-05	1.74E-05	1.48E-05	1.40E-05	1.31E-05				
Cumulative proportion	1.00E+00	1.00E+00	1.00E+00	1.00E+00	1.00E+00	1.00E+00				

SUPPLEMENTARY FIGURES

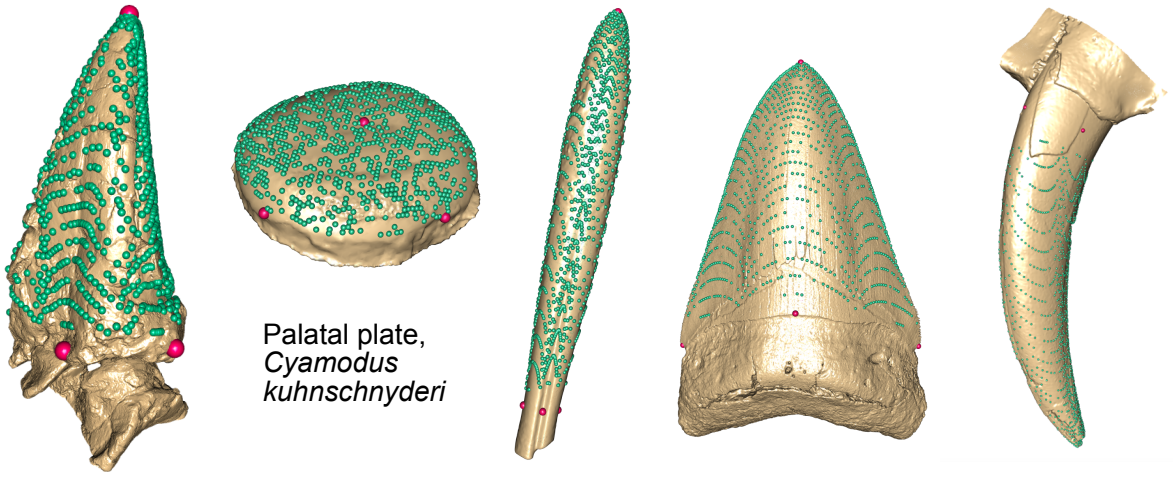

Fig. S1. Results of the patching procedure on other conical objects (not to scale). The sense of scale is given by the size of landmarks and semi-landmarks, which have a fixed size.

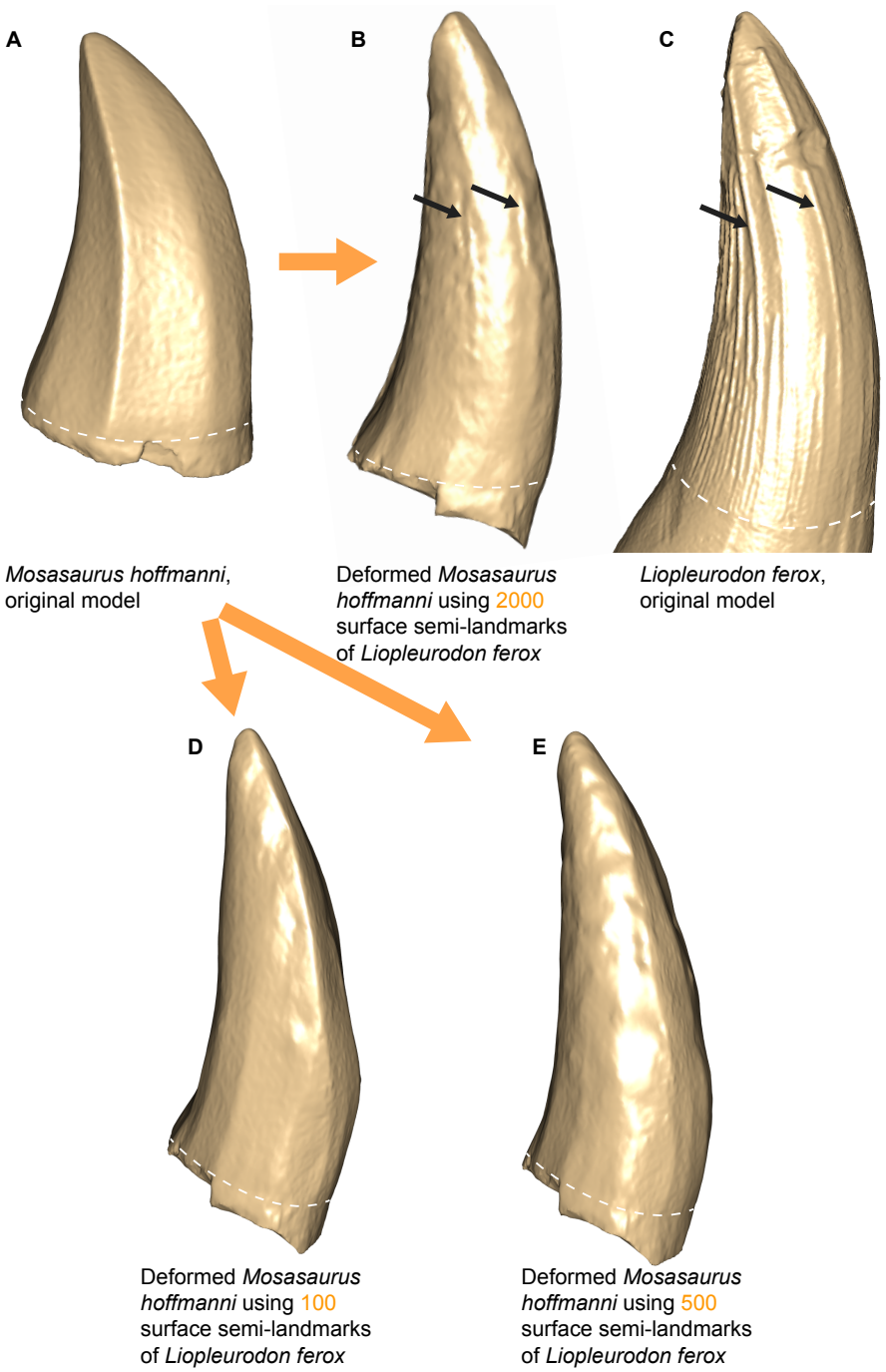

Fig. S2. Thin-plate spline deformation of the 3D mesh of Mosasaurus hoffmanni using the landmarks of Liopleurodon ferox. A, original model of the crown of the mosasaurid Mosasaurus hoffmanni. **B**, mesh of Mosasaurus hoffmanni deformed by using 2000 surface semi-landmarks sampled on the pliosaurid Liopleurodon ferox. **C**, original model of the crown of Liopleurodon ferox. **D**, **E**, meshes Mosasaurus hoffmanni deformed by using 100 and 500 surface semi-landmarks (respectively) sampled on the pliosaurid Liopleurodon ferox This example shows that the 2000 surface landmarks used forms a dense enough network that is able to capture (and hence be used to deform) the apicobasal ridges of pliosaurids (black arrow), among other structures, but still not the finer apicobasal ridglets. Not to scale; the white dotted line represents the basal limit of the zone sampled by landmarks.

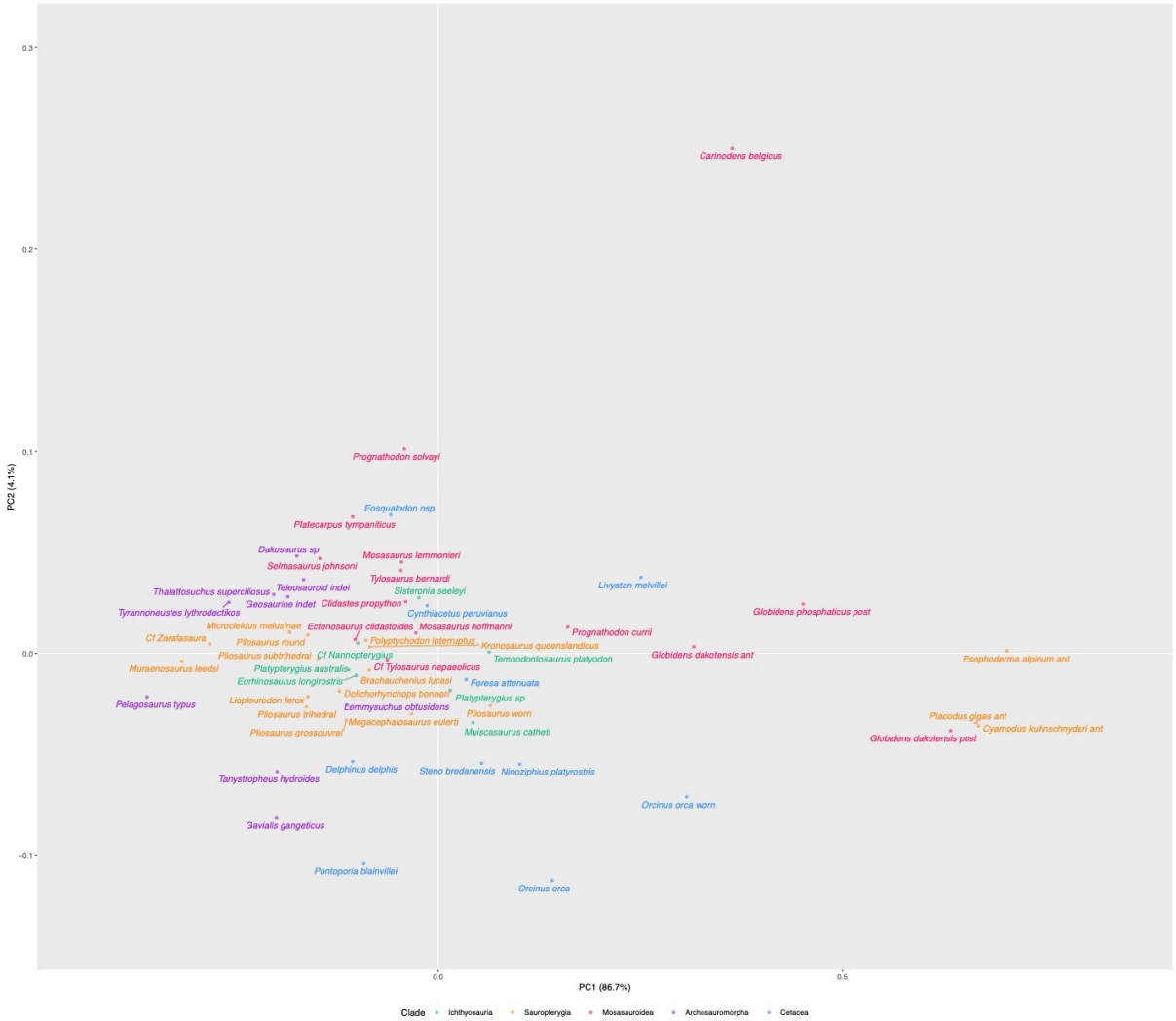

Fig. S3. Morphospace occupation (first two PCA axes) with all taxon names indicated.

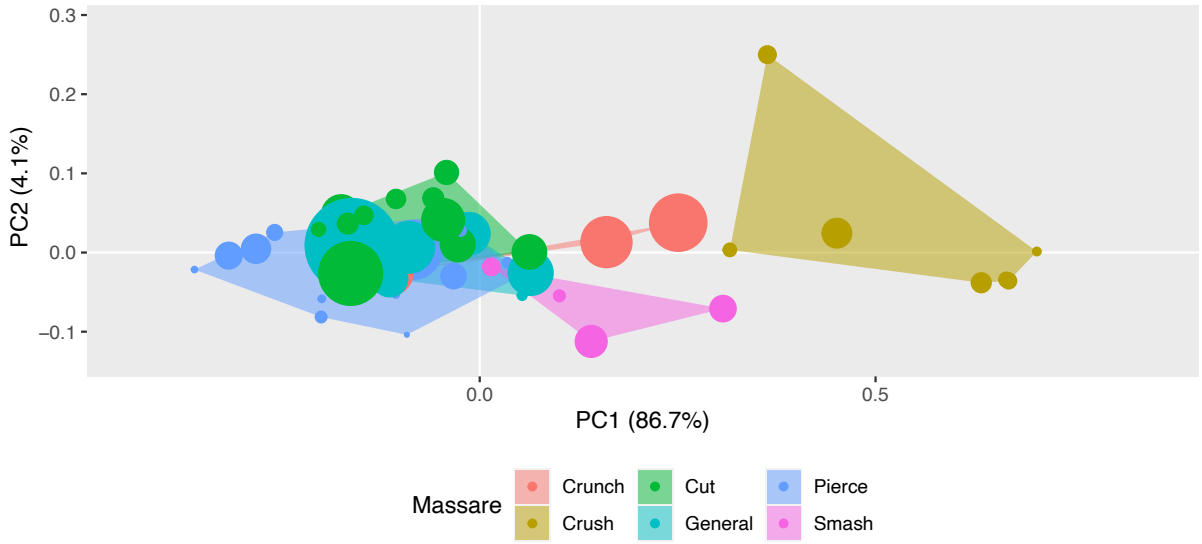

Fig. S4. Morphospace occupation with convex hulls representing Massare's guilds. The size of the dots is linearly correlated to centroid size.

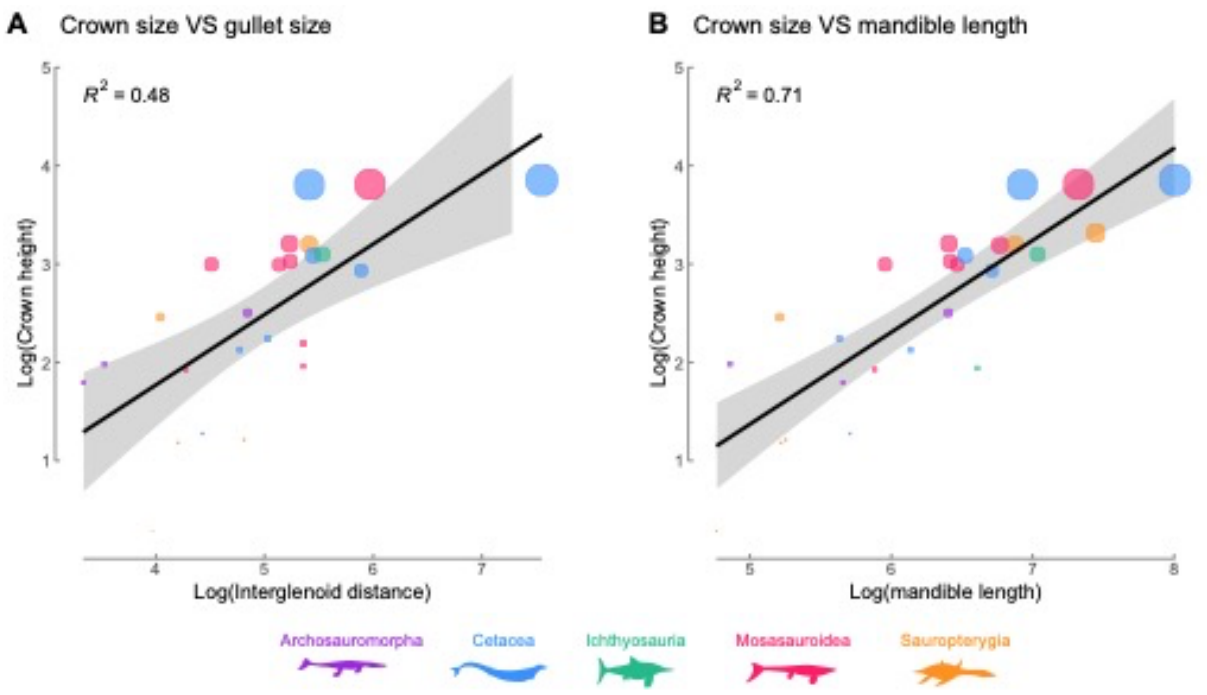

Fig. S5. Size regressions. A, log(crown size) VS log(gullet size). **B**, log(crown size) VS log(mandible length) (right panel).

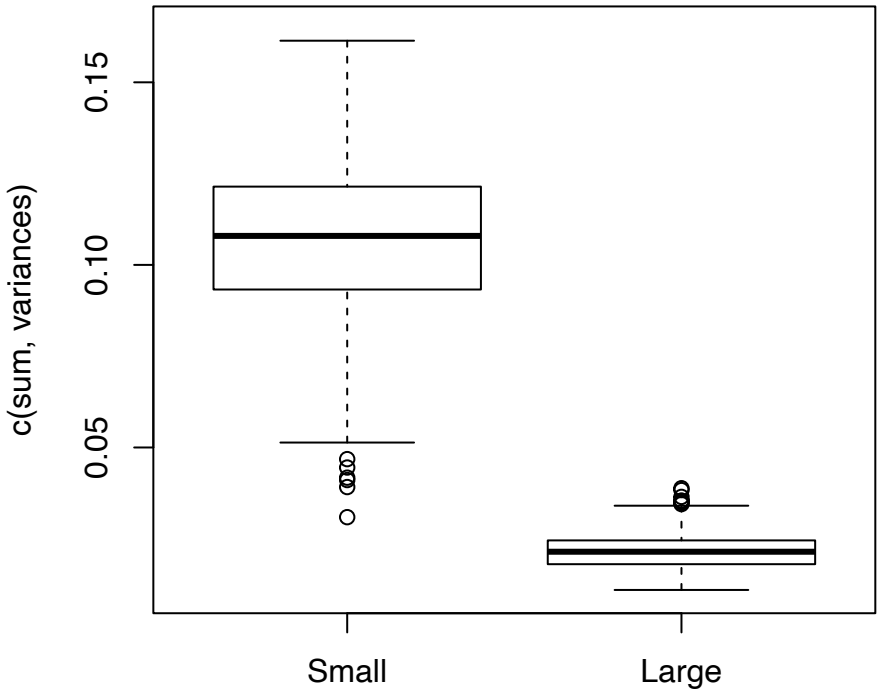

Fig. S6. Comparison of disparity between small (<20 mm) and large (>20 mm) crowns. Disparity was computed with the disparity v.1.6.8 package [9], using all axes of the PCA, 1000 bootstraps, and the sum of variance metric. The p-value of the Wilcoxon-Mann-Whitney comparing these two populations = 0.

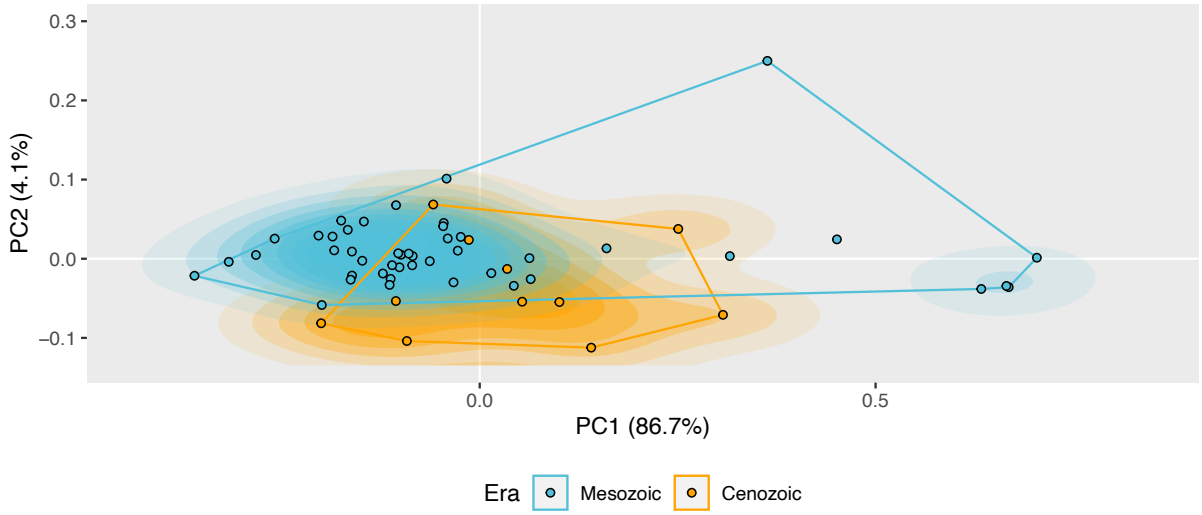

Fig. S7. Morphospace occupation with convex hulls (thin lines) and densities (shaded colors) separated by geological eras.

SUPPLEMENTARY TEXT

Step-by-step guide of the high-density geometric morphometric procedure

- Create a 3D dome composed of more than 2000 triangles.
- Gather 3D models of tooth crowns.
- In your software of choice (we used Stratovan Checkpoint v.20.10.13.0859), place five fixed landmarks on the dome and the tooth crowns, using a strict routine. Our sequence is the following: (i) apex, (ii) basolabial extremity of the crown, (iii) basolingual extremity of the crown, (iv) basodistal extremity of the crown, (v) basolingual extremity of the crown.
- The following procedure is fully automatic.
- Import the models and their fixed landmarks in the R statistical environment, using the stats and geomorph v4.0.3 [10,11].
- Sample the coordinates of the triangles composing the dome; this will provide automatically generated surface semi-landmarks; this part of the protocol is borrowed from pseudolandmarking techniques. We used 2000 surface semi-landmarks for this paper (see Fig. S2 for the outcome of less dense sampling procedures).
- Create the atlas and patch the dome and its surface semi-landmarks onto each tooth crown model with the Morpho v2.9 package [12].
- Run a Generalised Procrustes Superimposition (GPA) to eliminate the size and positioning factors and then a Principal Component analysis (PCA) on the GPA data to produce morphospaces, via geomorph v4.0.3 [11]. Centroid size can be used as a proxy for the original crown size.
- Compute density-based macroevolutionary landscape using PCA data, with the method explained in Fischer et al. [2].

Acknowledgments of curators and data handlers

We warmly thank Guillaume Duboys de Lavigerie + Pierre Sparla (Université de Liège, Belgium), Dr. Morgan Churchill (University of Wisconsin, USA), Dr. Ellen Coombs (Smithsonian Institute, Washington, USA), Michelle Johnston (Kronosaurus Korner, Australia), Fatima Khaldoune (Office Chérifien des Phosphates, Morocco), Matt Riley (Sedgwick Museum, UK), Dr. Torsten Scheyer (Universität Zürich, Switzerland), and Silvan Thüring (Naturmuseum Solothurn, Switzerland) for loaning specimens and/or providing 3D models. We also warmly thank curators John Ososky (Smithsonian Institute, Washington DC), Dr. Scott Hocknull + Kristen Spring + Joanne Wilkinson (Queensland Museum, Australia), Megan Sims + Anna Whitaker + Dr. Chris Beard (Kansas University, USA), Chase Shelburne + Dr. Laura Wilson (Sternberg Museum, Kansas, USA), Dr. Annelise Folie + Cecilia Cousin + Dr. Olivier

Pauwels (Royal Belgian Institute of Natural Sciences, Belgium) and Dr. Ben Thuy (Naturemusee, Luxembourg) for hosting us in their institutions.

REFERENCES

1. Evans AR et al. 2021 A universal power law for modelling the growth and form of teeth, claws, horns, thorns, beaks, and shells. BMC Biology **19**, 1–14. (doi:10.1186/s12915-021-00990-w)
2. Fischer V, Maclaren JA, Soul LC, Bennion RF, Druckenmiller PS, Benson RBJ. 2020 The macroevolutionary landscape of short-necked plesiosaurians. Sci Rep **10**, 1–12. (doi:10.1038/s41598-020-73413-5)
3. McCurry MR, Evans AR, Fitzgerald EMG, McHenry CR, Bevitt J, Pyenson ND. 2019 The repeated evolution of dental apicobasal ridges in aquatic-feeding mammals and reptiles. Biological Journal of the Linnean Society , In press. (doi:10.1093/biolinnean/blz025)
4. Lambert O, Bianucci G, Post K, de Muizon C, Salas-Gismondi R, Urbina M, Reumer J. 2010 The giant bite of a new raptorial sperm whale from the Miocene epoch of Peru. Nature **466**, 105–108.
5. Páramo-Fonseca ME, García-Guerrero J, Benavides-Cabra CD, Padilla-Bernal S, Castañeda-Gómez AJ. 2021 A benchmark specimen of Muiscasaurus catheti from the upper Aptian of Villa de Leiva, Colombia: New anatomical features and phylogenetic implications. Cretaceous Research **119**, 104685. (doi:https://doi.org/10.1016/j.cretres.2020.104685)
6. Peredo CM, Peredo JS, Pyenson ND. 2018 Convergence on dental simplification in the evolution of whales. Paleobiology **44**, 434–443. (doi:10.1017/pab.2018.9)
7. Ballell A, Moon BC, Porro LB, Benton MJ, Rayfield EJ. 2019 Convergence and functional evolution of longirostry in crocodylomorphs. Palaeontology , pala.12432. (doi:10.1111/pala.12432)
8. Spiekman SNF, Neenan JM, Fraser NC, Fernandez V, Rieppel O, Nosotti S, Scheyer TM. 2020 Aquatic Habits and Niche Partitioning in the Extraordinarily Long-Necked Triassic Reptile Tanystropheus. Current Biology , 1–7. (doi:10.1016/j.cub.2020.07.025)
9. Guillerme T. 2018 dispRity: A modular R package for measuring disparity. Methods in Ecology and Evolution **In Press**. (doi:10.1111/2041-210X.13022)
10. R Core Team. 2016 R: A language and environment for statistical computing.
11. Adams D, Collyer M, Kaliontzopoulou A. 2020 Geomorph: Software for geometric morphometric analyses.
12. Schlager S, Jefferis G, Dryden I. 2021 Morpho: calculations and visualisations related to geometric morphometrics.